Affibody Molecule for Positron Emission Tomography Imaging of Human Epidermal Growth Factor Receptor: Validation in Mouse Models and Human Cancer Tissues

Weizhi Chen
Harbin Medical University
Shuang Miao
Harbin Medical University
Yao Sun
Central China Normal University
Yang Liu
Harbin Medical University
Chunhe Wang
Harbin Medical University
Xiang Liu
Harbin Medical University
Zhen Cheng
Stanford University School of Medicine
Xilin Sun (sunxl@ems.hrbmu.edu.cn)
Harbin Medical University

Research

Keywords: Affibody molecules, EGFR, Ga-68, NSCLC, PET, Radionuclide imaging ClinicalTrials.gov ID NCT02916329

Posted Date: November 2nd, 2021

DOI: https://doi.org/10.21203/rs.3.rs-1024214/v1

Abstract

Background: Tumor heterogeneity and changes in epidermal growth factor receptor (EGFR) expression status over time post challenges for the design of strategies for effective anti-EGFR monoclonal antibodies in the treatment of non-small-cell lung cancer (NSCLC). Therefore, there is an urgent need to develop techniques for real-time and comprehensive tumor EGFR profiling especially in lung cancer precision medicine trials. Radionuclide imaging of EGFR expression in tumors may screen patients for EGFR-targeting therapies and predict response or resistance to certain treatments.

Methods: EGFR-specific Affibody molecule ($Z_{EGFR:1907}$) was radiolabeled with ^{68}Ga. The radioligands were characterized in vitro and in mice bearing subcutaneous tumors with varying levels of EGFR expression: HCC827 (EGFR overexpression), H1975 (moderate-high), A549 (moderate), H358 (low), and H520 (negative). In vivo tumor targeting activity using PET imaging and biodistribution were conducted in tumor-bearing nude mice. Autoradiography, western blot, immunofluorescence, and immunohistochemistry were performed in human tumor samples. Statistical analyses were performed using GraphPad Prism 7.0. One-way or two-way analysis of variance (ANOVA) followed by the Bonferroni's multiple comparisons test was used. Statistical significance was set at $P < 0.05$.

Results: ^{68}Ga-NOTA-$Z_{EGFR:1907}$ showed higher uptake in high EGFR-expressing cells (HCC827, H1975) when compared to cells with moderate to low EGFR (A549, H358) or without EGFR (H520). Radionuclide imaging showed probe accumulation was preferential in EGFR-expressing tumors, particularly in HCC827, H1975 xenografts. A549 and H358 xenografts were mildly and indistinctly visualized. EGFR-negative H520 xenografts were barely visible at any time-point. Biodistribution showed a significantly higher accumulation in HCC827 tumors when compared to H520 tumors (3.20 ± 0.10 %ID/g vs. 0.81 ± 0.08 %ID/g at 2h, $P< 0.05$). Specific binding to EGFR could be competitively blocked by excess un-radiolabeled affibody molecules in cell uptake, PET imaging and biodistribution assays. Autoradiography showed the regions with high radiotracer uptake partly overlapped with the area of positive EGFR immunofluorescence and immunohistochemistry. Finally, the overall accumulation of autoradiography was positively correlated with immunohistochemistry score.

Conclusion: Affibody-based radiotracer ^{68}Ga-NOTA-$Z_{EGFR:1907}$ is suitable for identification of EGFR expression, showing great potential for further applications and clinical translation.

Background

Epidermal growth factor receptor (EGFR), one of four members of ErbB family, is overexpressed in most human epithelial carcinomas(1) and plays a crucial role in oncogenic phenotypic transformation and maintenance, tumor angiogenesis, metastasis, and treatment resistance.(2–4) EGFR has emerged as a biomarker for diagnosis and prognosis as well as a therapeutic target for many cancers including breast cancer, non-small-cell lung cancer (NSCLC), head and neck squamous cell carcinoma (HNSCC), and bladder cancer.(5–8) Response to various EGFR-targeting therapeutic strategies of HNSCC and NSCLC is

associated with a high level of EGFR expression.(9, 10) Thus, the detection of EGFR expression level in malignant tumors can provide important prognostic and predictive information that can influence the choice of treatment for cancer patients.

Biopsy is a common method to determine the level of EGFR expression in human tumors. However, this methodology is associated with several problems, such as invasiveness, and sampling errors. Moreover, EGFR expression varies between primary and metastatic tumors,(11, 12) and may change over time or in response to therapy.(13) Visualization of EGFR expression using molecular imaging techniques, such as single photon emission computed tomography (SPECT) and positron-emission tomography (PET), and EGFR-specific probes can overcome many problems of biopsy-based methods. It is possible to simultaneously evaluate EGFR expression levels in both primary and metastatic tumors in this way. In addition, these imaging techniques can provide repetitive noninvasive determination of the level of EGFR expression in tumors. The use of these techniques would substantially improve the management of cancer patients.

Several types of imaging probes, such as based on epidermal growth factor (EGF),(14, 15) anti-EGFR monoclonal antibody,(16–18) and antibody fragments,(19, 20) have been studied as diagnostic and prognostic markers. The major issue with the use of antibody-based probes for imaging is their slow clearance from blood and nonspecific compartments, which requires several days to obtain an acceptable imaging contrast.

Affibody molecules are very promising targeting proteins for the development of radionuclide imaging probes in vivo. Affibody molecules are small scaffold proteins with a three-helix bundle structure based on the Z-domain derived from one of the IgG-binding domains of staphylococcal protein A.(21, 22) Affibody-based probes are excellent for tumor-targeted imaging in vivo(23–26) owing to their small size and molecular weight (6-7 kDa), high stability and binding specificity, affinity,(22, 23) excellent tumor tissue penetration and accumulation, and rapid clearance rate from the blood. Moreover, the structure of affibody molecules can potentially be site-specifically modified (27). Anti-human ErbB2 (HER2) affibody molecules (Z_{HER2}) and their derivatives have been successfully radiolabeled with various radionuclides and safely used to visualize HER2-expressing tumors in animal models(28–30) and patients with metastatic breast cancer.(31–33) However, to date radiolabeled anti-human EGFR affibody molecules have never been used in noninvasive imaging of tumors in patients. Thus, based on previous studies we aimed to further develop clinically translatable affibody probes to use as tumor biomarkers for radionuclide imaging.

Anti-EGFR affibody proteins with high affinity (in nanomolar range) and no cross-binding to other growth factor receptors(22) have been reported, such as $Z_{EGFR:1907}$(22, 34), and used in imaging and drug delivery in xenograft models in preclinical research.(35) Here, we conjugated an affibody derivative, Ac-Cys-$Z_{EGFR:1907}$ (Ac-CVDNKFNKEMWAAWEEIRNLPNLNGWQMTAFIASLVDDPSQSANLLAEA-KKLNDAQAPK-NH2, with 59 amino acid residues and a cysteine at the N terminal, can be site-specifically conjugated through the cysteine residue)(36, 37) with a bifunctional chelator, MMA-NOTA (1,4,7-triazacyclononane-

N,N',N''-triacetic acid maleimidoethylmonoamide), for labeling with Gallium-68 (^{68}Ga, $T_{1/2}$ = 67.6 min, β^+ abundance 90%, E β^+max = 1880 keV) and used this EGFR-targeted radiotracer, ^{68}Ga-NOTA-$Z_{EGFR:1907}$, to assess EGFR expression in xenograft models of NSCLC using positron emission tomography (PET). Furthermore, to determine the clinical translational ability of the radiotracer, we evaluated its ability to recognize EGFR in clinical NSCLC tumor samples. In addition, we also carried out experimental studies in gastric cancer and colorectal cancer specimens, so as to expand the application range of the radiotracer.

Methods

Radiosynthesis of ^{68}Ga-NOTA-$Z_{EGFR:1907}$

Anti-EGFR affibody molecule (Ac-Cys-$Z_{EGFR:1907}$) synthesized on an automatic peptide synthesizer (CS Bio, CS 336X)(38) were site-specifically conjugated with bifunctional chelator MMA-NOTA (CheMatech Inc., Dijon, France) through cysteine residue at the N terminal as previously described(39). The resulting bioconjugate, Ac-Cys(NOTA)-$Z_{EGFR:1907}$, was abbreviated as NOTA-$Z_{EGFR:1907}$. 100 μg of NOTA-$Z_{EGFR:1907}$ were resuspended in 250 μL of 0.38 M sodium acetate, followed by 1 mL of 0.05 M HCl with $^{68}GaCl_3$ solution generated from an ^{68}Ge/^{68}Ga generator (ITG GmbH, Germany). The mixture was heated (80°C, 15 min, pH 3.5-4.0) in an iQS®Ga-68 fluidic labeling module and passed through a Sep-Pak® Light C18 column (Waters Corporation, Milford, Massachusetts USA), and the radiolabeled product, ^{68}Ga-NOTA-$Z_{EGFR:1907}$, was eluted with 70% alcohol and passed through a 0.22-μm Millipore filter (Millex®GP, Merck) into a sterile vial. Then, the product was purified by radio-HPLC (Gilso, GX-281) with a protein-and-peptide C4 column (Grace Vydac 214TP54, Columbia, Maryland) using a gradient system of solvent A (0.1% TFA/H2O) and solvent B (0.1%TFA/MeCN).

Octanol/Water Distribution Coefficient

The distribution coefficient was measured in an octanol and phosphate buffered saline (PBS) system. ^{68}Ga-NOTA-$Z_{EGFR:1907}$ (~370 kBq, 10 μCi) of 500 μL of PBS was added to 500 μL of octanol and mixed sufficiently for 0.5 h at room temperature, then centrifuged at 3000 rpm for 5 min. Aliquots (200 μL) were taken from each layer, and counted using a γ-counter (PerkinElmer 2480). The distribution coefficient was expressed as log D = $\log_{10}$(counts in octanol/counts in PBS) (mean ± SD, n = 5).

In Vitro and In Vivo Stability

^{68}Ga-NOTA-$Z_{EGFR:1907}$ (3.7 MBq, 100 μCi) was incubated with mouse serum (500 μL, Sigma-Aldrich) for 0 h, 1 h or 2 h at 37°C. At each time point, 0.74-1.48 MBq (20-40 μCi) solution was precipitated with 300 μL of ethanol and centrifuged (Eppendorf 5415R) at 16,000g for 2 min. The supernatant was transferred to a new Eppendorf, and dimethylformamide (300 μL, Sigma-Aldrich) was added to precipitate the residue of serum protein. After centrifugation, the supernatant was acidified with 300 μL of buffer A (water + 0.1% trifluoroacetic acid) and filtered through a 0.22-μm Millipore filter. The filtrate was then analyzed by the

radio-HPLC (Gilso, GX-281) under conditions identical to those used for analyzing the original radiolabeled affibody, obtained the HPLC chromatograms.

In vivo stability was performed in HCC827 tumor-bearing mice (n = 3), which were injected with ^{68}Ga-NOTA-$Z_{EGFR:1907}$ (11.1 MBq, 300 μCi, 100μL) via tail vein and euthanized 1 h afterward. Blood added with ethylene-diamine-tetra-acetic acid (EDTA, Sigma-Aldrich) was centrifuged (3000 rpm, 10 min) immediately after collection to remove blood cells. The plasma portions and tumors were homogenized (T18 digital ULTRA-TURRAX®, IKA) respectively with 500 μL of dimethylformamide with 1% Triton X-100 (Sigma-Aldrich). The next step was the same as in vitro stability.

Cell Culture

Five NSCLC cell lines were selected: HCC827 (high EGFR expression), H1975 (moderate-high), A549 (moderate), H358 (low), and H520 (negative EGFR). All cell lines were purchased form American Type Culture Collection (Manassas, Virginia) and cultured as previously reported.(40)

Cellular Uptake and Efflux

^{68}Ga-NOTA-$Z_{EGFR:1907}$ cellular uptake and blocking with non-radiolabeled NOTA-$Z_{EGFR:1907}$, as well as efflux were performed at 15, 30, 60, and 120 min as previously reported.(40)

Animal Xenograft Models

All animal experiments were approved by the Harbin Medical University Animal Ethics Committee in accordance with Chinese legislation and followed relevant guidelines. The institutional review board approved this study on mice with NSCLC tumor xenografts. Female BALB/c nude mice (n = 14 for HCC827 group; n = 4 for H1975, A549, or H358 group; n = 7 for H520 group, total of 33) (from the Shanghai Slack Experimental Animal Center of qualified animals SCXK) aged 4-5 weeks and weighed 18-22 g were implanted subcutaneously with HCC827, H1975, A549, H358, or H520 cells (5×10^6) in right shoulder. Tumor size was measured by caliper every other day until reaching a volume of 250 mm^3 or a diameter of 10 mm (approximately 4-6 weeks). If volume exceeded 500 mm^3, the tumor was discarded.

PET/CT Imaging and Biodistribution

PET/CT imaging of tumor-bearing mice was performed on a clinical time-of-light (TOF) 64-slice PET/CT scanner (Discovery 790 Elite, GE Healthcare). The mice bearing tumors (n = 8 for HCC827 group; n = 4 for H1975, A549, H358 or H520 group) were intravenously injected with 3.7 MBq (100 μCi, 100μL) of ^{68}Ga-NOTA-$Z_{EGFR:1907}$ via a tail vein. At 30 min, 60 min and 120 min after injection, the mice were anesthetized with 2% isourane and scanned immediately. Between each scan, mice were woken up to empty the bladder. With the help of a laser beam attached to the scanner, mice were placed prone and near the center of the field of view of the scanner, and 3-min static scans were obtained. The images were reconstructed on a 512 × 512 matrix for a 15-cm-diameter field of view by a two-dimensional ordered subsets expectation maximization (OSEM) algorithm and visualized with Advantage Workstation version AW4.6 software package (GE Healthcare). For each scan, regions of interests (ROIs) were drawn over the

tumor and major organs on decay-corrected whole-body coronal images. The radioactivity concentrations (accumulations) within the tumor and muscle were obtained from mean pixel values within the multiple ROI volumes and then converted to megabecquerels per milliliter per minute using the calibration factor determined for the PET system. These values were then divided by the administered activity to obtain (assuming a tissue density of 1 g/ml) an image ROI-derived percent injected dose per gram (%ID/g). All the images decay-corrected to the time point of radiotracer injection.

For ex vivo biodistribution experiments, tumor-bearing mice were sacrificed by cervical dislocation after imaging.(40) Major organs or tissues were harvested and weighed. The radioactivity of those was measured using a γ-counter, and calibrated against a known aliquot of the injection and normalized with tissue weight from each organ. The radioactivity uptake in organs or tissues was expressed as %ID/g.

For blocking study, equivalent amount of ^{68}Ga-NOTA-$Z_{EGFR:1907}$ (3.7 MBq, 100 μCi, 100μL) spiked with non-radiolabeled affibody (500 μg) was injected intravenously into HCC827 tumor mice (n=4) for PET imaging and biodistribution.

Western Blot and Immunofluorescence

Western blot and immunofluorescence experiments were performed as previously reported(40). The concentration of anti-EGFR primary antibody (#4267, Cell Signaling Technology) was 1:1,000 for western blot and 1:50 for immunofluorescence. Antibodies for immunofluorescence staining, green = Alexa Fluor® Plus 488, blue = DAPI.

Immunohistochemistry

EGFR protein expression was determined by immunohistochemistry (IHC) as described previously(41) and scored visually using Fromowitz positive cell semi-quantitative classification. EGFR positive expression was localized to the cell membrane and distributed evenly in light yellow or tan granules. EGFR expression score was calculated according to the percentage of positive staining cells and staining intensity. The scoring criteria for the percentage of positive staining cells was as follows: 0 to 5% = 0; 6 to 25% = 1; 26 to 50% = 2; 51 to 75% = 3; >75% = 4. Staining intensity was graded as follows: absent or faint blush = 0; pale yellow = 1; brown-yellow = 2; tan = 3. When two integrals were added, the integral ≤ 1 meant negative (-) and when the score was ≥ 2 points, it was considered positive (+). Specifically, 2-3 points corresponded to weakly positive (+), 4-5 points to moderately positive (++), and 6-7 points to strongly positive (+++).

Toxicity Assay

In vivo toxicity of ^{68}Ga-NOTA-$Z_{EGFR:1907}$ was tested with mice bearing HCC827 or H520 xenografts using necropsy (18-25 g, n = 3). Typically, ^{68}Ga-NOTA-$Z_{EGFR:1907}$ (14.8 MBq, 400 μCi, 150μL per day) was injected via tail vein for five consecutive days. An equal volume of normal saline was injected into the control group. On the sixth day, the mice were sacrificed by cervical dislocation and the major organs were stained with hematoxylin and eosin (H&E).

Autoradiography

Tumor samples from 31 solid tumor patients with NSCLC, gastric or colorectal cancer between February and May 2019 were collected fresh within 1 h of resection. Tumors were embedded within optimal-cutting-temperature compound, and froze at -80°C. Autoradiography, H&E and immunofluorescence staining were performed on consecutive tumor sections. Sections were placed in a small box containing a solution of ^{68}Ga-NOTA-$Z_{EGFR:1907}$ in PBS (74kBq/mL). The mixture was shaken for 1 h at room temperature. After incubation, sections were rinsed thrice in ice-cold PBS followed by exposure to photoreceptive film for 6 h and then imaged with a Cyclone Plus storage phosphor system (PerkinElmer). The intensity of radioactivity was expressed as digital light units (DLU) per mm^2. The study has been approved by the Medical Ethical Committee of Harbin Medical University and Harbin Medical University Institutional Review Board, and all subjects signed an informed consent form, and registered individually (ClinicalTrials.gov ID NCT02916329).

Statistical Analysis

To assess the association between ^{68}Ga-NOTA-$Z_{EGFR:1907}$ uptake and EGFR expression status, we performed statistical analyses in four ways: (i) Welch's t test was used to compare quantitative data between two independent samples (EGFR-expressing negative and positive); (ii) for comparisons involving more than two categories, one-way or two-way ANOVA, followed by Bonferroni's multiple comparison test, was performed; and (iii) correlations were conducted using the best-fit linear regression line (GraphPad prism 7.0); and (iv) a receiver operating characteristic (ROC) curve was drawn with a gray scale value, thereby evaluating the ability to discriminate EGFR expression status and identifying the optimum ^{68}Ga-NOTA-$Z_{EGFR:1907}$ autoradiography gray scale cut-off value using the maximum Youden's index (sensitivity + specificity – 1). The total AUC and its 95% CI were calculated. Statistical significance was set at $P < 0.05$. Quantitative values were expressed as means ± SD as indicated.

Results

Radiochemistry and Characterization

Radiolabeling was complete in 15 min (Figure 1A), with high radiochemical yields (RCY of 65%) and radiochemical purity (RCP ≥ 95%). ^{68}Ga-NOTA-$Z_{EGFR:1907}$ showed a retention time of 10.7 min and specific activity of approximately 9.6×10^3 MBq/μmol. From octanol/water distribution coefficient measurements, the log *D* value was determined to be -1.16 ± 0.12, indicating the radiolabeled affibody was water-soluble. Moreover, stability assay showed that the radiotracer had good stability both in vitro and in vivo (Figure 1B-F).

In Vitro Assays of Cells and Xenografts

Confirmed by western blot, HCC827 cells and xenografts have the highest level of EGFR expression, whereas H1975 of moderate to high levels, A549 of moderate levels, H358 of low levels, and H520 of

undetectable EGFR expression (Figure 2A-B, Figure S1-S2). Similarly, a significantly stronger fluorescence signal was observed by immunostaining in HCC827 cells and xenografts, moderate in 549, whereas signal was negligible in H520 (Figure S1-S2). Immunohistochemistry revealed strong staining in HCC827 xenografts, whereas H1975, A549, and H358 xenografts showed different degrees of regional positive staining. Moreover, H520 xenografts showed no detectable EGFR expression (Figure S2).

Cell Uptake and Efflux Assays

To demonstrate that the binding of probe to target occurs only at physiological temperature, cell uptake and efflux assays were conducted at 37°C or 4°C within an incubation period of 15-120 min (Figure 2C-F). At 37°C, ^{68}Ga-NOTA-$Z_{EGFR:1907}$ rapidly accumulated in HCC827 cells at 15 min (4.06 ± 0.28 %), peaking at 120 min (9.03 ± 0.61 %). The accumulation of ^{68}Ga-NOTA-$Z_{EGFR:1907}$ was significantly higher in HCC827 cells than H1975, A549, H358, or H520 cells (5.31 ± 0.12 %, 4.18 ± 0.05 %, 2.60 ± 0.23 %, and 1.19 ± 0.46 %, respectively) at 120 min ($P < 0.0001$). ^{68}Ga-NOTA-$Z_{EGFR:1907}$ activity was approximately nine-fold lower at 4˚C when compared with 37˚C at all time points, indicating specific binding occurred at physiological temperature, maybe internalization also helped. Pre-incubation with a large amount of nonradioactive affibody molecules (NOTA-$Z_{EGFR:1907}$) significantly ($P < 0.0001$) inhibited ^{68}Ga-NOTA-$Z_{EGFR:1907}$ uptake in HCC827 cells at 37℃. This demonstrated that the binding could be saturated, which is evidence of the EGFR-specific binding.

To study the cellular retention of radioactivity after interrupted incubation of radiolabeled affibody molecules, cultured NSCLC cells were incubated for 2 h at 37C. The results showed that retention of ^{68}Ga-NOTA-$Z_{EGFR:1907}$ in HCC827 cells eventually decreased, it remained significantly higher than any other cells ($P < 0.0001$).

In Vivo PET Imaging

^{68}Ga-NOTA-$Z_{EGFR:1907}$ provided effective PET imaging of different EGFR-expressing levels tumors (Figure 3A-B). HCC827 xenografts were clearly delineated by the radiotracer starting at 30 min, with excellent tumor imaging quality at later time points (2.58 ± 0.15 and 2.69 ± 0.14 %ID/g at 1 and 2 h). Similarly, H1975 xenografts also showed distinct ^{68}Ga-NOTA-$Z_{EGFR:1907}$ accumulation in tumors, allowing clear tumor imaging (2.04 ± 0.20 %ID/g at 2 h) and good tumor-to-background contrast. A549 and H358 xenografts were mildly and indistinctly visualized at 2 h (1.56 ± 0.15 and 1.40 ± 0.11 %ID/g, respectively). H520 xenografts were barely visible by PET at any time point (0.90 ± 0.12 %ID/g at 2 h). In addition to the tumor, high radioactivity accumulation was also observed in the liver, kidney, and bladder of all the xenograft mice. ^{68}Ga-NOTA-$Z_{EGFR:1907}$ was mainly cleared through the renal-urine system (67.86 ± 3.53 %ID/g from 30 to 120 min), and blood uptake dropped dramatically from 30 min, (9.19 ± 0.57 vs. 4.31 ± 0.22 %ID/g at 30 and 120 min, respectively). When a large number of excess nonlabelled affibody molecules were co-injected into mice bearing HCC827 xenografts, tumor uptake of ^{68}Ga-NOTA-$Z_{EGFR:1907}$ was barely visible at any time point. The tumor size data at imaging were shown in Figure S3A ($P < 0.05$),

then tumor-bearing mice were euthanatized and tumors were harvested for western blot. Quantification analysis of PET images showed that tumor uptakes and tumor-to-muscle ratios were significantly different between tumor models with various EGFR expression levels and mice bearing HCC827 xenografts (Figure S3B-C, $P < 0.05$), suggesting that ^{68}Ga-NOTA-$Z_{EGFR:1907}$ has high sensitivity to EGFR.

Correlation Study

The value of cell uptake in vitro and quantitative analysis of tumor uptake of PET images in vivo of ^{68}Ga-NOTA-$Z_{EGFR:1907}$ at different time points were then plotted against the relative EGFR expression levels measured by western blot (normalized against GAPDH). The plots revealed that at any time, there was an excellent correlation between cell uptake value and western assay (% of applied activity vs. EGFR level, $R^2 > 0.92$, $P < 0.01$) (Figure S4A). A good correlation was achieved when the tumor uptake value (mean %ID/g of ^{68}Ga-NOTA-$Z_{EGFR:1907}$) was used for analysis ($R^2 \geq 0.87$, $P < 0.05$) (Figure S4B).

Biodistribution

Biodistribution assays showed that ^{68}Ga-NOTA-$Z_{EGFR:1907}$ strongly accumulated in HCC827 tumors (3.20 ± 0.10 %ID/g at 2 h) (Figure 3C, Table S1). Compared with HCC827 tumors, the accumulation of probe in H1975, A549, H358 or H520 tumors was statistically different (2.06 ± 0.06, 1.49 ± 0.04, 1.17 ± 0.10, and 0.81 ± 0.08 %ID/g at 2 h, respectively). The liver and kidney biodistribution patterns in five tumor models were similar, with high probe uptake. Moderate radioactivity was detected in blood, with lower intensity than the above organs. There was an endogenous and low expression of EGFR in a number of healthy tissues. The tumor-to-normal-tissue ratios, including tumor/lung, tumor/blood, tumor/muscle, tumor/liver, tumor/kidney, and tumor/bone ratios, were significantly different between HCC827 and any other tumor-bearing mouse model. Blocking experiment revealed a remarkable decline in overall uptake of ^{68}Ga-NOTA-$Z_{EGFR:1907}$, except kidney. Specifically, tumor uptake in HCC827 xenografts decreased markedly from 3.20 ± 0.10 to 0.67 ± 0.08 %ID/g (79% inhibition, $P < 0.0001$), and liver also significantly reduced from 12.48 ± 1.60 to 5.41 ± 0.54 %ID/g (57% inhibition, $P < 0.0001$), further demonstrating EGFR-targeting specificity of ^{68}Ga-NOTA-$Z_{EGFR:1907}$.

Toxicity assay

Biotoxicity assay is essential to assess the feasibility of radiolabeled probes for biological application. H&E staining was performed to examine whether ^{68}Ga-NOTA-$Z_{EGFR:1907}$ induced morphological changes in tissues. There were no significant morphological differences between lung, liver, kidney, and spleen of mice injected with ^{68}Ga-NOTA-$Z_{EGFR:1907}$ or saline solution (Figure S5).

^{68} Ga-NOTA-Z $_{EGFR:1907}$ allows monitoring of EGFR expression in human solid tumor samples

To determine the translational potential of ^{68}Ga-NOTA-$Z_{EGFR:1907}$ for clinical application, we assessed the binding ability of ^{68}Ga-NOTA-$Z_{EGFR:1907}$ to fresh human solid tumor tissues (Figure 4, Figure S6-S7). The

results revealed ^{68}Ga-NOTA-$Z_{EGFR:1907}$ preferentially accumulated in high EGFR-expressing tumors, whereas no accumulation other than background signal was found in low EGFR-expressing tumors, demonstrating that ^{68}Ga-NOTA-$Z_{EGFR:1907}$ specifically bound to EGFR-positive tumors.

Clinicopathological data were summarized accordingly in Table 1. The positive EGFR-expressing rate was 88.2% (15 of 17) for NSCLC, 66.7% (6 of 9) for gastric cancer, and 100% (5 of 5) for colorectal cancer. The gray scale value of ^{68}Ga-NOTA-$Z_{EGFR:1907}$ in human tissue samples increased linearly with EGFR expression, scored by IHC in the area confirmed by H&E (R^2 = 0.62, P < 0.0001) (Figure 5A).

Table 1
Patient characteristics.

Characteristics	Total	IHC scores +++	IHC scores ++	IHC scores +	IHC scores -
Patients, n **(%)**	31	10 (32.3)	10 (32.3)	6 (19.4)	5 (16.0)
Ages (years)					
Median	65	65	65	66	63
Range	50-77	54-75	58-75	51-77	50-75
Sex (male/female)	14:17	7:3	1:9	3:3	3:2
Histology, n **(%)**					
Stomach	9	2 (22.2)	3 (33.3)	1 (11.1)	3 (33.3)
Adenocarcinoma	8	2	3	1	2
Mixed carcinoma	1	0	0	0	1
Colorectum	5	1 (20)	4 (80)	0	0
Adenocarcinoma	5	1	4	0	0
Lung	17	7 (41.2)	3 (17.6)	5 (29.4)	2 (11.8)
Adenocarcinoma	12	5	3	4	0
Squamous cell carcinoma	4	2	0	1	1
Mucoepidermoid carcinoma	1	0	0	0	1

EGFR protein expression was determined using immunohistochemistry (IHC) and scored using Fromowitz positive cell semi-quantitative classification. Negative (-) means IHC scores ≤ 1 point; weakly positive (+) means 2-3 points; moderate positive (++) means 4-5 points; strongly positive (+++) means 6-7 points.

The sensitivity and specificity of predicting EGFR expression were obtained by ROC curve for the gray values of autoradiography of the EGFR positive group and the EGFR negative group confirmed by H&E staining and immunohistochemistry. When EGFR expression was very low (0-1 point), there was 100% agreement between the IHC staining and autoradiography (gray scale < 1.99×10^6 DLU/mm^2, sensitivity of 77%, and specificity of 100%, Figure 5B-C). Thus, 1.99×10^6 DLU/mm^2 was set as the cutoff value for detecting EGFR expression. When EGFR expression was weak (2-3 points), a wide range of gray scale values were observed, from 0.09×10^6 DLU/mm^2 to 2.35×10^6 DLU/mm^2 (Figure 5D). Finally, in moderate-high EGFR expression (4-7 points), there was 95% agreement between IHC staining and autoradiography, whose gray scale values were almost always greater than 2.42×10^6 DLU/mm^2 (sensitivity of 90%, and specificity of 100%).

Discussion

Molecular imaging has played a role of great importance in noninvasive detection and quantification of EGFR expression in clinical research.(16, 42–44) PET is an imaging method that can provide superior sensitivity and quantitation accuracy compared to SPECT(45). Gallium-68 is a suitable positron-emitting radionuclide for clinical PET imaging. The merits of this radionuclide include the good availability of gallium-68 because of generator production and short half-life of 67.6 min, which results in low absorbed dose burden to patients. These advantages are conducive to clinical translation and underpin the remarkable expansion of clinical research with gallium-68 labeled radiopharmaceuticals, especially the ones based on rapidly cleared proteins(46).

We found that ^{68}Ga-NOTA-$Z_{EGFR:1907}$ only focused on the expression of EGFR protein and the uptake of that was merely correlated with total protein expression of EGFR (the order of uptake in tumor-bearing mice: HCC827 > H1975 > A549 > H358 > H520). However, the probe was not associated with EGFR mutants. Such results are consistent with the principle of targeted binding of ^{68}Ga-NOTA-$Z_{EGFR:1907}$. As we all know, EGFR is a single-chain transmembrane glycoprotein comprising an extracellular ligand-binding domain, a transmembrane region, and an intracellular tyrosine kinase domain. $Z_{EGFR:1907}$ is specifically bound to the extracellular segment of EGFR, and it cannot bind to the intracellular tyrosine kinase domain. Therefore, the degree of intracellular mutation of EGFR could not be distinguished.

Anti-EGFR affibody $Z_{EGFR:1907}$ has a similar molecular weight to epidermal growth factor (EGF) (7 kDa vs. 6.4 kDa). However, compared with ^{68}Ga-labeled EGF-based radiotracers, ^{68}Ga-NOTA-$Z_{EGFR:1907}$ was higher in tumor uptake (1.51±0.16 vs. 2.07±0.73 %ID/g) at 30min p.i..(47) Moreover, tumor accumulations of ^{18}F-FBEM-cEGF in UM-SCC1 xenografts were 1.87 ± 0.44 and 0.98 ± 0.33 %ID/g at 60 and 120 min p.i. respectively(14), while that of ^{68}Ga-NOTA-$Z_{EGFR:1907}$ were higher (2.58 ± 0.15 and 2.69 ± 0.14 %ID/g at 60 and 120 min p.i.). These results indicate that affibody-based radiotracer exhibits an extended retention time compared to EGF-based radiotracers.

In view of the biological half-life of antibodies is very long, such as that of cetuximab is 65 to 95 hours in the blood(48), a radioactive tracer with long half-life is needed to visualize its uptake, resulting in an increase in the patient's radiation dose. As for ^{68}Ga-NOTA-$Z_{EGFR:1907}$, both physical half-life of Gallium-68 and biological half-life of affibody are shorter and suitable for clinical application. Moreover, given that probe accumulation in tumors depends on physiological characteristics such as vascular permeability, tumors with high EGFR expression do not necessarily exhibit high uptake of radiolabeled antibodies.(49–51) In addition, ^{89}Zr-labeled affibody demonstrated specific uptake in EGFR-expressing tissues, also tumor-to-organ ratio of that was higher compared with ^{89}Zr-labeled antibody.(52)

The accumulations of ^{68}Ga-NOTA-$Z_{EGFR:1907}$ in most organs were lower except liver and kidney, mainly attributed to the fact that they are the major organs responsible for metabolism and clearance. More importantly, it is known that the high natural expression of EGFR in the liver. Liver accumulation of ^{68}Ga-NOTA-$Z_{EGFR:1907}$ was slightly lower in HCC827 tumor models compared to ^{64}Cu-DOTA-$Z_{EGFR:1907}$.(38) The unbound probe is rapidly cleared from blood via the kidneys, which makes it possible to obtain high contrast images after only a few hours after injection(53). Low ^{68}Ga-NOTA-$Z_{EGFR:1907}$ uptake in the lung region was detected, which was consistent with low endogenous EGFR expression reported in this organ.(54) Importantly, low accumulation in lung offers the considerable advantage of this probe in identifying primary or metastatic lung tumors expressing EGFR. Despite large injection mass of ^{68}Ga-NOTA-$Z_{EGFR:1907}$, no pathological changes were detected in the liver, kidneys, spleen, or lungs in biotoxicity assays, indicating that ^{68}Ga-NOTA-$Z_{EGFR:1907}$ is safe and therefore suitable for clinical applications.

Notably, ^{68}Ga-NOTA-$Z_{EGFR:1907}$ could not detect very low (0-1 point) EGFR-expressing tumors. In tumors with weak (2-3 points) EGFR expression, ^{68}Ga-NOTA-$Z_{EGFR:1907}$ accumulations were also slightly high, without completely correlation with IHC scores. Thus, it is possible that a minimum threshold of EGFR expression is required for reliably detecting EGFR levels with the radiotracer. In remaining moderate-high EGFR-expressing tumors (4-7 points), IHC scores and gray scale values were both significantly elevated. Taken together, our results indicate that a radiotracer-based gray scale value of $\leq 1.99 \times 10^6$ DLU/mm^2 may be used as cutoff value to rule-out low EGFR-expressing tumors patient subgroups. Moreover, based on the IHC staining results, a cutoff value of $\geq 2.42 \times 10^6$ DLU/mm^2 may identify moderate to high EGFR-expressing tumors. Besides, these cutoff values should be considered as exploratory, on account of that our study was based on a small sample. Finally, there were overlaps between the areas stained by EGFR antibodies and those detected by ^{68}Ga-NOTA-$Z_{EGFR:1907}$ in tissue samples, further demonstrating that the radiotracer specifically binds to EGFR in human tissues.

Although in vivo subcutaneous transplant tumor models provide extremely valuable information, future preclinical researches using orthotopic inoculation models, as well as clinical studies for ^{68}Ga-NOTA-$Z_{EGFR:1907}$ PET imaging in patients, are necessary for the clinical translation of this probe. Our data from this pilot study were limited, nevertheless, they provide a proof-of-principle of the clinical potential of ^{68}Ga-NOTA-$Z_{EGFR:1907}$ for PET imaging and quantifying EGFR expression in human tumors, and for

monitoring the efficacy of EGFR-targeted therapy, such as anti-EGFR monoclonal antibodies cetuximab and panitumumab.(55)

Conclusions

We have successfully site-specifically radiolabeled anti-EGFR affibody Ac-Cys-$Z_{EGFR:1907}$ and ^{68}Ga with high radiochemical yield used in molecular imaging. ^{68}Ga-NOTA-$Z_{EGFR:1907}$ has favorable EGFR-targeted characterization in vitro and excellent tumor imaging quality in vivo. It is proved that ^{68}Ga-NOTA-$Z_{EGFR:1907}$ binds to EGFR in human cancer tissue specimens validated by EGFR antibodies. Thus, ^{68}Ga-NOTA-$Z_{EGFR:1907}$ shows great clinical translation potential for screening responsive patients during EGFR-targeted therapy.

Abbreviations

ATCC
American Type Culture Collection
AUC
area under the curve
CPM
counts per minute
DLU
digital light units
EDTA
ethylenediaminetetraacetic acid
EGF
epidermal growth factor
EGFR
epidermal growth factor receptor
H&E
hematoxylin and eosin
HNSCC
head-neck squamous cell carcinoma
IHC
immunohistochemistry
NOTA
1,4,7-triazacyclononane-1,4,7-triacetic acid
NSCLC
non-small-cell lung cancer
OSEM
ordered subsets expectation maximization

PBS
phosphate buffered saline
PET
positron emission tomography
ROC
receiver operating characteristic
ROI
region of interest
HPLC
high performance liquid chromatography
RT
room temperature
SDS-PAGE
sodium dodecyl sulfate polyacrylamide gel electrophoresis
TOF
time-of-flight
%ID/g
percentage injected radioactive dose (decay corrected) per gram of tissue.

Declarations

Ethical approval and consent to participate

The specimens of patients with solid tumor were conducted with permission from the Medical Ethical Committee of Harbin Medical University and Harbin Medical University Institutional Review Board. All animal studies were carried out in compliance with the China Guidelines for Animal Care and Ethic for Animal Experiments and the experimental protocols were approved by the Animal Use and Care Committee of Harbin Medical University.

Consent for publication

Not applicable

Availability of data and materials

The dataset supporting the conclusions of this article is included within the article and its additional file.

Competing interests

The authors declare that they have no conflict interests.

Funding

This work was supported by the National Natural Science Foundation of China (81627901), Natural Science Foundation of Heilongjiang Province (Grant No. JQ2020H002), the Tou-Yan Innovation Team Program of the Heilongjiang Province (2019-15), National Basic Research Program of China (2015CB931800) and the Key Laboratory of Molecular Imaging Foundation (College of Heilongjiang Province).

Author's Contributions

Weizhi Chen: conceptualization, data curation, formal analysis, investigation, methodology, software, validation, visualization, and writing – original draft. Shuang Miao: conceptualization, data curation, methodology, and validation. Yao Sun: validation. Yang Liu: validation. Chunhe Wang: validation. Xiang Liu: validation. Zhen Cheng: resources and writing – review & editing. Xilin Sun: conceptualization, funding acquisition, project administration, resources, supervision, and writing – review & editing. All authors read and approved the final manuscript.

Acknowledgements

Not applicable

Clinical trial registration number

ClinicalTrials.gov ID NCT02916329

References

1. Ciardiello F, Tortora G. A novel approach in the treatment of cancer: targeting the epidermal growth factor receptor. Clinical Cancer Research. 2001;7(10):2958–70.
2. Nicholson RI, Gee JM, Harper ME. EGFR and cancer prognosis. Eur J Cancer. 2001;37 Suppl 4:S9-15.
3. Lo HW, Hsu SC, Aliseyed M, Gunduz M, Xia W, Wei Y, et al. Nuclear interaction of EGFR and STAT3 in the activation of the iNOS/NO pathway. Cancer Cell. 2005;7(6):575.
4. Riesterer O, Milas L, Ang KK. Use of Molecular Biomarkers for Predicting the Response to Radiotherapy With or Without Chemotherapy. Journal of Clinical Oncology Official Journal of the American Society of Clinical Oncology. 2007;25(26):4075–83.
5. Tsutsui S, Kataoka A, Ohno S, Murakami S, Hachitanda Y. Prognostic and predictive value of epidermal growth factor receptor in recurrent breast cancer. Clinical Cancer Research An Official Journal of the American Association for Cancer Research. 2002;8(11):3454.
6. Selvaggi, G. Epidermal growth factor receptor overexpression correlates with a poor prognosis in completely resected non-small-cell lung cancer. Annals of Oncology. 2004;15(1):28–32.
7. Atif AH, Fida HZ, Saher A, Muhammad I, Yousuf KE, Samreen N, et al. Immunohistochemical expression of epidermal growth factor receptor (EGFR) in South Asian head and neck squamous cell

carcinoma: association with various risk factors and clinico-pathologic and prognostic parameters. World Journal of Surgical Oncology. 2018;16(1):118-.

8. Hashmi AA, Hussain ZF, Irfan M, Khan EY, Faridi N, Naqvi H, et al. Prognostic significance of epidermal growth factor receptor (EGFR) over expression in urothelial carcinoma of urinary bladder. Bmc Urology. 2018;18(1).
9. Pirker R, Pereira JR, Pawel JV, Krzakowski M, Ramlau R. EGFR expression as a predictor of survival for first-line chemotherapy plus cetuximab in patients with advanced non-small-cell lung cancer: analysis of data from the phase 3 FLEX study. Lancet Oncology. 2012;13(1):33.
10. Bentzen, S. M. Epidermal growth factor receptor expression in pretreatment biopsies from head and neck squamous cell carcinoma as a predictive factor for a benefit from accelerated radiation therapy in a randomized controlled trial. Journal of Clinical Oncology. 2005;23(24):5560–7.
11. Wei Q, Shui Y, Zheng S, Wester K, Nordgren H, Nygren P, et al. EGFR, HER2 and HER3 expression in primary colorectal carcinomas and corresponding metastases: Implications for targeted radionuclide therapy. Oncology Reports. 2011;25(1):3–11.
12. Kang H, Kiess A, Chung CH. Emerging biomarkers in head and neck cancer in the era of genomics. Nature Reviews Clinical Oncology. 2014;12(1):11–26.
13. Oude Munnink TH, de Vries EG, Vedelaar SR, Timmer-Bosscha H, Schröder CP, Brouwers AH, et al. Lapatinib and 17AAG reduce 89Zr-trastuzumab-F(ab')2 uptake in SKBR3 tumor xenografts. Mol Pharm. 2012;9(11):2995–3002.
14. Li W, Gang N, Lang L, Ning G, Ying M, Kiesewetter DO, et al. PET imaging of EGF receptors using [18F]FBEM-EGF in a Head and Neck Squamous Cell Carcinoma model. European Journal of Nuclear Medicine & Molecular Imaging. 2012;39(2):300–8.
15. Haibiao, Gong, Joy, Kovar, Lael, Cheung, et al. A comparative study of affibody, panitumumab, and EGF for near-infrared fluorescence imaging of EGFR- and EGFRvIII-expressing tumors. Cancer Biology & Therapy. 2014.
16. Nishio N, Berg NSvd, Keulen Sv, Martin BA, Fakurnejad S, Zhou Q, et al. Optimal Dosing Strategy for Fluorescence-Guided Surgery with Panitumumab-IRDye800CW in Head and Neck Cancer. Molecular Imaging and Biology. 2020;22(1):156–64.
17. Manivasagan P, Nguyen VT, Jun SW, Hoang G, Oh J. Anti-EGFR antibody conjugated thiol chitosan-layered gold nanoshells for dual-modal imaging-guided cancer combination therapy. Journal of Controlled Release. 2019;311–312.
18. Wan-I, Kuo, Kai-Hung, Cheng, Ya-Jen, Chang, et al. Radiolabeling, Characteristics and NanoSPECT/CT Imaging of 188Re-cetuximab in NCI-H292 Human Lung Cancer Xenografts. Anticancer Research. 2019.
19. Dijk LK, Van, Boerman OC, Franssen GM, Jasper L, Kaanders JHAM, Johan B. Early response monitoring with 18F-FDG PET and cetuximab-F(ab')2-SPECT after radiotherapy of human head and neck squamous cell carcinomas in a mouse model. Journal of Nuclear Medicine. 2014;55(10):1665–70.

20. Dirk Bauerschlag, Ivo Meinhold-Heerlein, Nicolai Maass, Andreas Bleilevens, Karen Bräutigam, Wa'el Al Rawashdeh, et al. Detection and Specific Elimination of EGFR$^+$ Ovarian Cancer Cells Using a Near Infrared Photoimmunotheranostic Approach. Pharmaceutical Research. 2017.
21. Nord K, Gunneriusson E, Ringdahl J, Ståhl S, Uhlén M, Nygren P. Binding proteins selected from combinatorial libraries of an |[alpha]|-helical bacterial receptor domain. Nature Biotechnology. 1997;15(8):772.
22. M F, Nordberg E, Höidén-Guthenberg I, Brismar H, Adams GP, Nilsson FY, et al. Phage display selection of Affibody molecules with specific binding to the extracellular domain of the epidermal growth factor receptor. Protein Engineering Design & Selection. 2007;20(4):189–99.
23. Cheng Z, De Jesus OP, Namavari M, De A, Levi J, Webster JM, et al. Small-animal PET imaging of human epidermal growth factor receptor type 2 expression with site-specific 18F-labeled protein scaffold molecules. Journal of Nuclear Medicine Official Publication Society of Nuclear Medicine. 2008;49(5):804–13.
24. Hoppmann S, Miao Z, Liu S, Liu H, Ren G, Bao A, et al. Radiolabeled affibody-albumin bioconjugates for HER2-positive cancer targeting. Bioconjugate Chemistry. 2011;22(3):413.
25. Samkoe KS, Sardar HS, Bates BD, Tselepidakis NN, Gunn JR, Hoffer-Hawlik KA, et al. Preclinical imaging of epidermal growth factor receptor with ABY-029 in soft-tissue sarcoma for fluorescence-guided surgery and tumor detection. Journal of Surgical Oncology. 2019.
26. pieve cd, Makarem A, Turnock S, Maczynska J, Kramer-Marek G. Thiol-Reactive PODS-Bearing Bifunctional Chelators for the Development of EGFR Targeting [18F]AlF-Affibody Conjugates. Molecules. 2020;25:1562.
27. Nord K, Nilsson J, Nilsson B, Uhlén M, Nygren P. A combinatorial library of an α-helical bacterial receptor domain. Protein Eng. 1995;8(6):601–8.
28. Lubberink, M., L?fblom, J., Honarvar, H., et al. 188Re-ZHER2:V2, a promising affibody-based targeting agent against HER2-expressing tumors: Preclinical assessment. Journal of Nuclear Medicine. 2014.
29. Sörensen J, Velikyan I, Sandberg D, Wennborg A, Feldwisch J, Tolmachev V, et al. Measuring HER2-Receptor Expression In Metastatic Breast Cancer Using [68Ga]ABY-025 Affibody PET/CT. Theranostics. 2016;6(2):262–71.
30. Qi S, Hoppmann S, Xu Y, Cheng Z. PET Imaging of HER2-Positive Tumors with Cu-64-Labeled Affibody Molecules. Molecular Imaging & Biology. 2019.
31. Jens SR, Dan S, Mattias SM, Anders W, Joachim F, Vladimir T, et al. First-in-human molecular imaging of HER2 expression in breast cancer metastases using the 111In-ABY-025 affibody molecule. Journal of Nuclear Medicine. 2014;55(5):730–5.
32. Sandström M, Lindskog K, Velikyan I, Wennborg A, Feldwisch J, Sandberg D, et al. Biodistribution and radiation dosimetry of the anti-HER2 Affibody molecule 68Ga-ABY-025 in breast cancer patients. Journal of Nuclear Medicine. 2016;57(6).
33. Alhuseinalkhudhur A, Lubberink M, Lindman H, Tolmachev V, Srensen J. Kinetic analysis of HER2-binding ABY-025 Affibody molecule using dynamic PET in patients with metastatic breast cancer.

EJNMMI Research. 2020;10(1):21.

34. Friedman M, Orlova A, Johansson E, Eriksson TL, Höidén-Guthenberg I, Tolmachev V, et al. Directed evolution to low nanomolar affinity of a tumor-targeting epidermal growth factor receptor-binding affibody molecule. Journal of Molecular Biology. 2008;376(5):1388–402.
35. Wang Y, Telmer CA, Schmidt BF, Franke JD, Ort S, Arndtjovin D, et al. Fluorogen Activating Protein–Affibody Probes:Modular, No-Wash Measurement of Epidermal Growth Factor Receptors. Bioconjugate Chemistry. 2015;26(1):137.
36. Yang M, Cheng K, Qi S, Liu H, Jiang Y, Jiang H, et al. Affibody modified and radiolabeled gold-iron oxide hetero-nanostructures for tumor PET, optical and MR imaging. Biomaterials. 2013;34(11):2796–806.
37. Zhao P, Yang X, Qi S, Liu H, Jiang H, Hoppmann S, et al. Molecular Imaging of Hepatocellular Carcinoma Xenografts with Epidermal Growth Factor Receptor Targeted Affibody Probes. Biomed Research International. 2013;2013(1):759057-.
38. Zheng M, Gang R, Liu H, Lei J, Zhen C. Small-Animal PET Imaging of Human Epidermal Growth Factor Receptor Positive Tumor with a 64Cu Labeled Affibody Protein. Bioconjugate Chemistry. 2010;21(5):947–54.
39. Su X, Cheng K, Jeon J, Shen B, Venturin GT, Hu X, et al. Comparison of Two Site-Specifically 18F-Labeled Affibodies for PET Imaging of EGFR Positive Tumors. Molecular Pharmaceutics. 2014;11(11):3947–56.
40. Song Y, Xiao Z, Wang K, Wang X, Zhang C, Fang F, et al. Development and Evaluation of18F-IRS for Molecular Imaging Mutant EGF Receptors in NSCLC. Scientific Reports. 2017;7(1):3121.
41. Ruiz MI, Galleges, Floor K,., Steinberg SM, Grünberg K, ., Thunnissen FBJM, Belien JAM, et al. Combined assessment of EGFR pathway-related molecular markers and prognosis of NSCLC patients. British Journal of Cancer. 2009;100(1):145–52.
42. Catharina Willemien M-vdHvO, Gootjes EC, Huisman MC, Vugts DJ, Chantal R, Anne Marije L, et al. 89Zr-cetuximab PET imaging in patients with advanced colorectal cancer. Oncotarget. 2015;6(30):30384–93.
43. Makris NE, Ronald B, Arthur VL, Lammertsma AA, Dongen GAMS, Van, Verheul HM, et al. PET/CT-derived whole-body and bone marrow dosimetry of 89Zr-cetuximab. Journal of Nuclear Medicine Official Publication Society of Nuclear Medicine. 2015;56(2):249–54.
44. Zhao C, Miao J, Shen G, Li J, Shi M, Zhang N, et al. Anti-Epidermal Growth Factor Receptor (EGFR) Monoclonal Antibody combined with Cisplatin and 5-Fluorouracil in Patients with Metastatic Nasopharyngeal Carcinoma after Radical Radiotherapy: A Multicentre, Open-label, Phase II Clinical Trial. Annals of Oncology. 2019.
45. Rahmim A, Zaidi H. PET versus SPECT: strengths, limitations and challenges. Nuclear Medicine Communications. 2008;29(3):193.
46. Velikyan I. Prospective of 68Ga-Radiopharmaceutical Development. Theranostics. 2014;4(1):47–80.

47. Velikyan I, Sundberg AL, Lindhe O, Höglund AU, Eriksson O, Werner E, et al. Preparation and evaluation of (68)Ga-DOTA-hEGF for visualization of EGFR expression in malignant tumors. Journal of Nuclear Medicine Official Publication Society of Nuclear Medicine. 2005;46(11):1881–8.
48. Fracasso PM, Rd BH, Arquette MA, Govindan R, Gao F, Wright LP, et al. A phase 1 escalating single-dose and weekly fixed-dose study of cetuximab: pharmacokinetic and pharmacodynamic rationale for dosing. Clinical Cancer Research An Official Journal of the American Association for Cancer Research. 2007;13(3):986–93.
49. Milenic DE, Wong KJ, Baidoo KE, Ray GL, Garmestani K, Williams M, et al. Cetuximab: preclinical evaluation of a monoclonal antibody targeting EGFR for radioimmunodiagnostic and radioimmunotherapeutic applications. Cancer Biotherapy & Radiopharmaceuticals. 2008;23(5):619.
50. Niu G, Li Z, Xie J, Le QT, Chen X. PET of EGFR antibody distribution in head and neck squamous cell carcinoma models. Journal of Nuclear Medicine. 2009;50(7):1116–23.
51. Aerts HJ, Dubois L, Perk L, Vermaelen P, van Dongen GA, Wouters BG, et al. Disparity between in vivo EGFR expression and 89Zr-labeled cetuximab uptake assessed with PET. Journal of Nuclear Medicine. 2009;50(1):123–31.
52. Garousi J, Andersson KG, Mitran B, Pichl ML, Ståhl S, Orlova A, et al. PET imaging of epidermal growth factor receptor expression in tumours using 89Zr-labelled ZEGFR:2377 affibody molecules. International Journal of Oncology. 2016;48(4):1325–32.
53. Krasniqi A, D'Huyvetter M, Devoogdt N, Frejd FY, Tolmachev V. Same-day imaging using small proteins: Clinical experience and translational prospects in oncology. Journal of Nuclear Medicine Official Publication Society of Nuclear Medicine. 2018;59(6).
54. Real FX, Rettig WJ, Chesa PG, Melamed MR, Old LJ, Mendelsohn J. Expression of epidermal growth factor receptor in human cultured cells and tissues: relationship to cell lineage and stage of differentiation. Cancer Research. 1986;46(9):4726.
55. Vallböhmer D, Lenz HJ. Epidermal Growth Factor Receptor as a Target for Chemotherapy. Clin Colorectal Cancer. 2005;5:S19-S27.

Figures

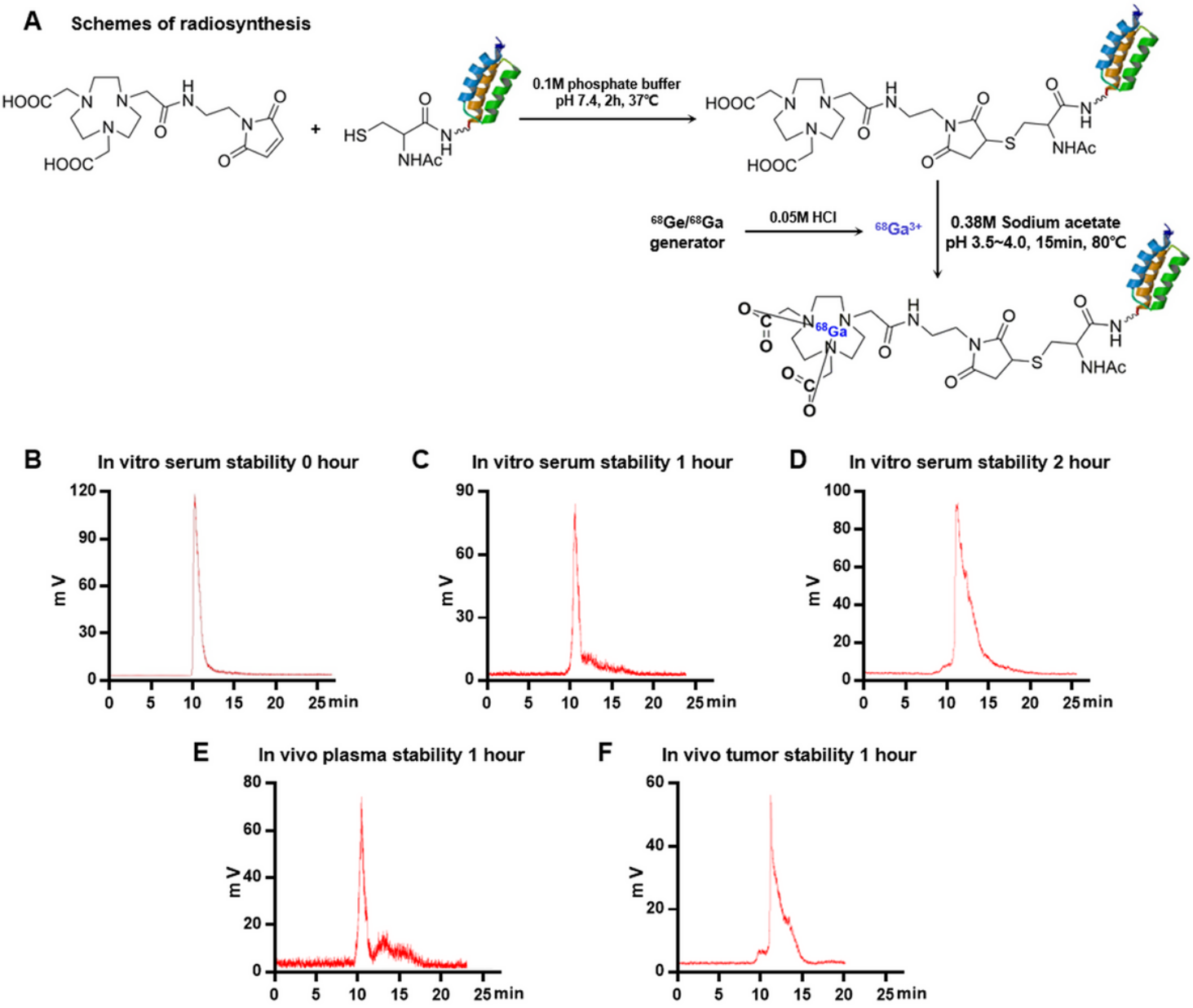

Figure 1

Schemes of radiosynthesis and stability of 68Ga-NOTA-ZEGFR:1907. (A) Schemes of radiosynthesis of 68Ga-NOTA-ZEGFR:1907. In vitro stability assay of 68Ga-NOTA-ZEGFR:1907 after incubation in mouse serum for 0 h (B), 1 h (C) and 2 h (D) by radio-HPLC. In vivo stability assay of 68Ga-NOTA-ZEGFR:1907 from samples of plasma (E) and tumor (F) at 1 h after injection via tail vein by radio-HPLC.

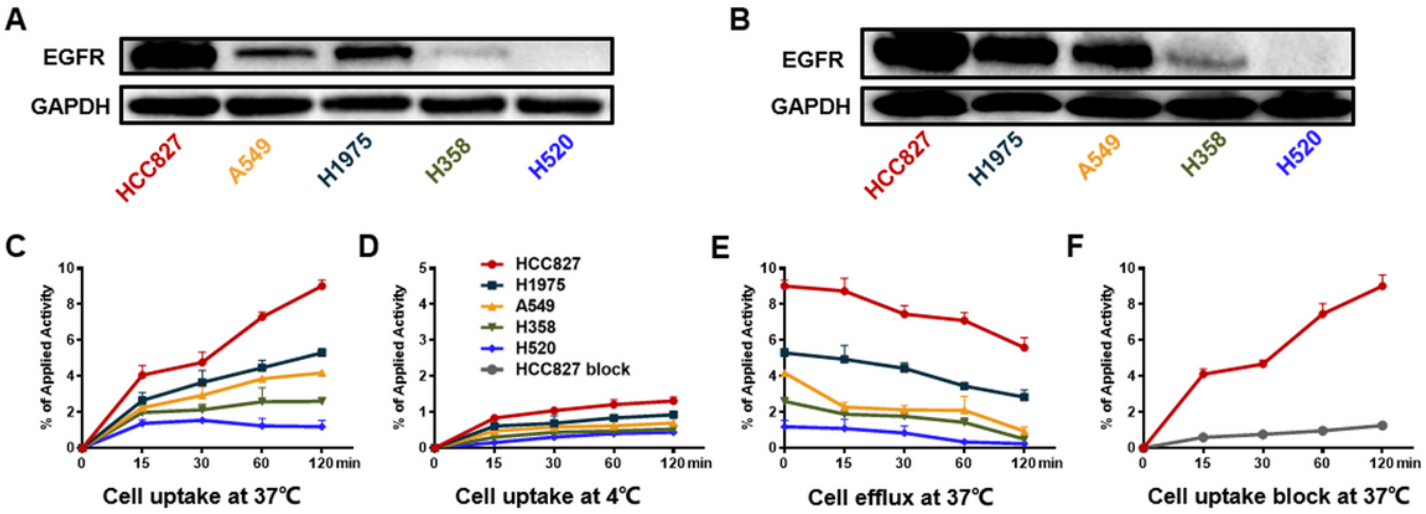

Figure 2

Cell line characterization and in vitro cell assay. Western blot quantification of EGFR expression at various NSCLC cell lines (A) and excised tumors (B), including HCC827, H1975, A549, H358 and H520 cells. GAPDH served as a reference for equal loading. Cell uptake (C, D) and efflux (E) of 68Ga-NOTA-ZEGFR:1907 in HCC827, H1975, A549, H358 and H520 cells over time at 37℃ (C, E) or 4℃ (D), and with or without the presence of nonradioactive affibody molecules ZEGFR:1907 in HCC827 cells (F). All results are expressed as the mean of triplicate measurements ± standard deviation.

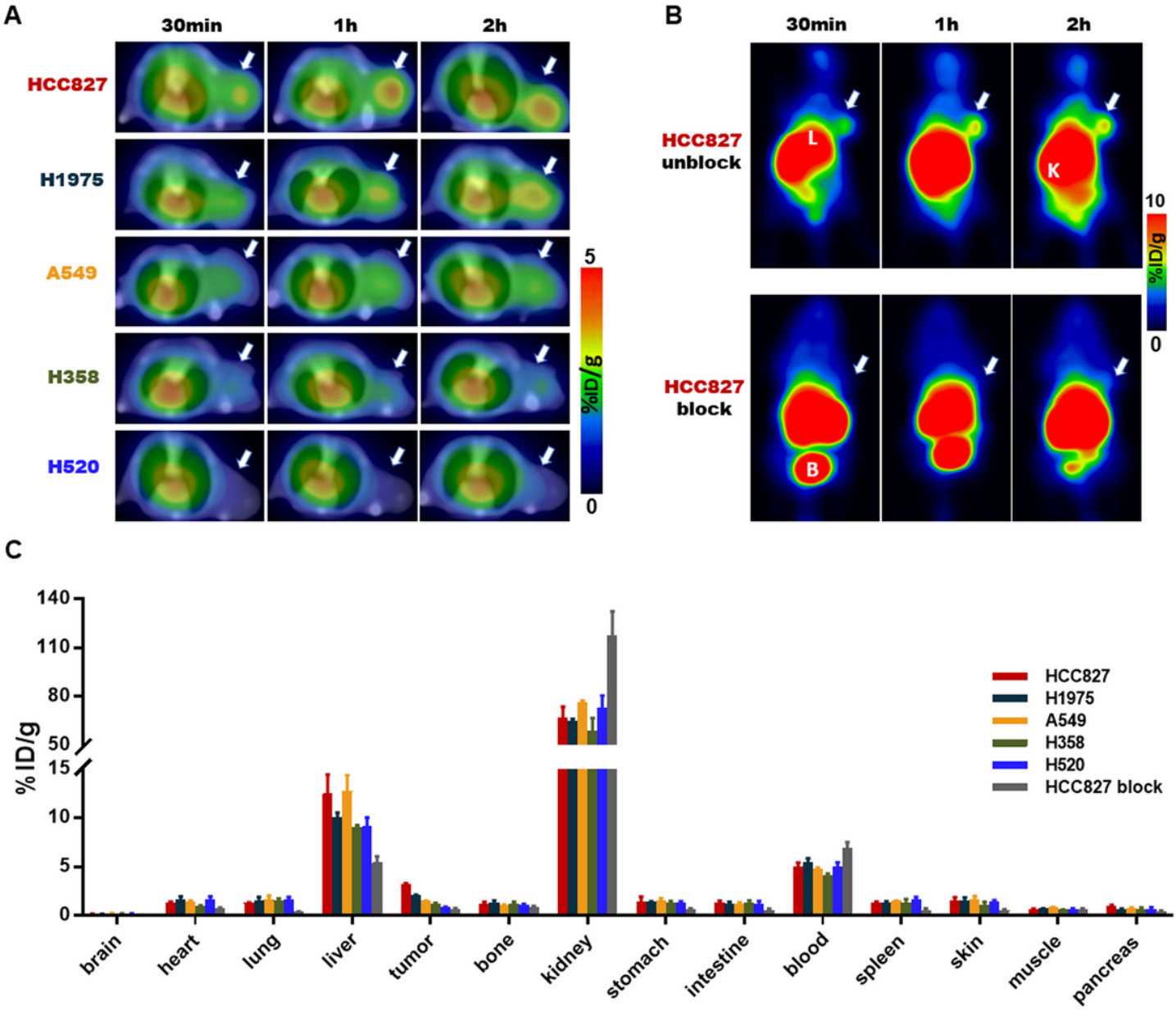

Figure 3

PET/CT imaging and biodistribution of NSCLC xenograft models. (A) Representative decay-corrected axial PET images of xenograft models at 30 min, 1 h, and 2 h after injection of 68Ga-NOTA-ZEGFR:1907 (3.7 MBq, 100 μCi). Arrows indicate the location of tumors. (B) Representative decay corrected coronal PET images of nude mice bearing HCC827 xenografts co-injected with 0 μg, or 500 μg (blocking dose) of cold affibody (ZEGFR:1907) at 30 min, 1 h, and 2 h after injection (3.7 MBq, 100 μCi). L: liver, K: kidney, B: bladder. (C) Ex vivo biodistribution of 68Ga-NOTA-ZEGFR:1907 (1.9-2.6 MBq per mouse) in HCC827, H1975, A549, H358, and H520 tumor-bearing nude mice (n = 4 per group) at 2 h after injection, and co-injection with 500 μg (blocking dose) of cold affibody (NOTA-ZEGFR:1907) in HCC827 tumor-bearing nude mice (n = 4) at 2 h after injection. Columns mean %ID/g; Error bars indicate the mean ± S.D.

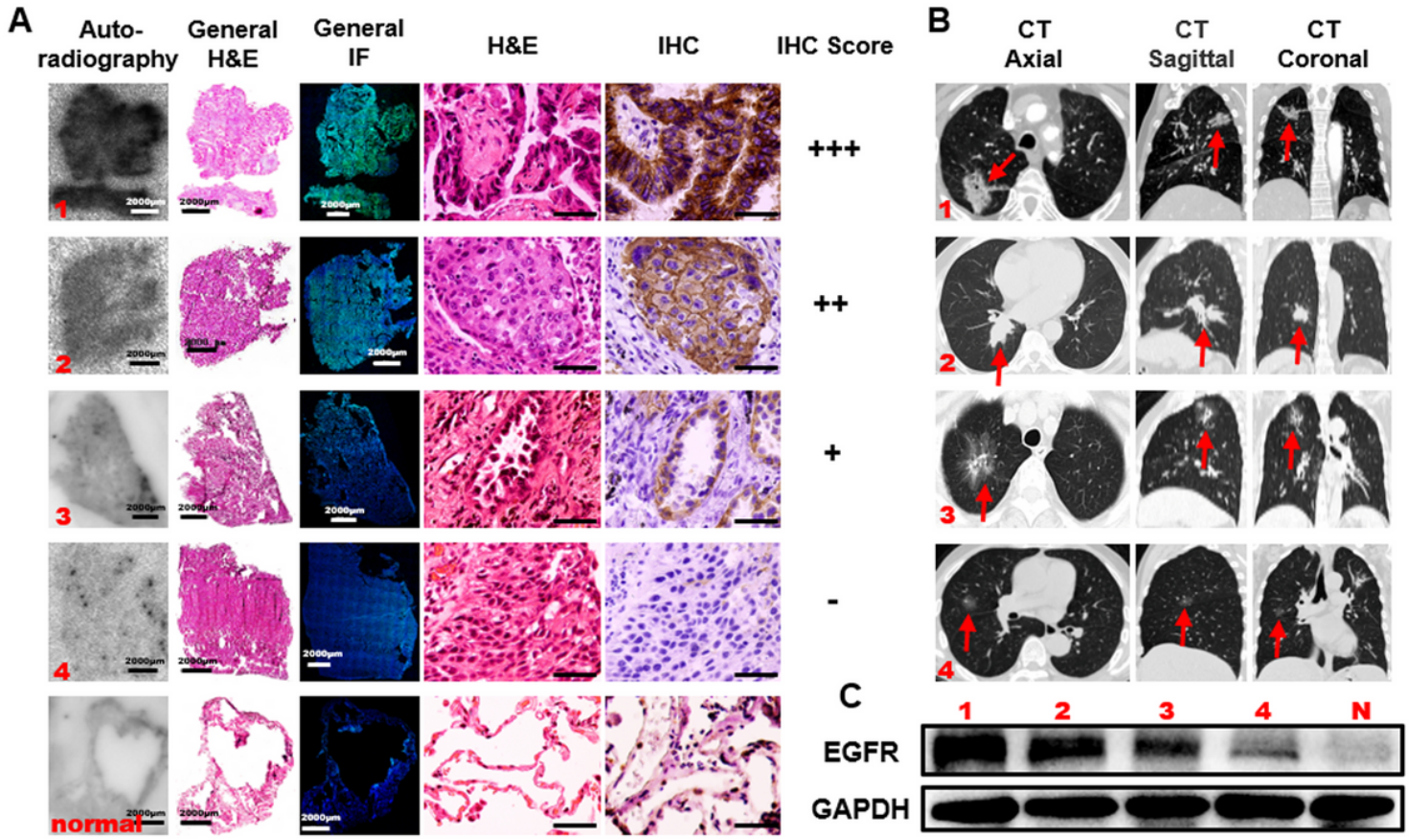

Figure 4

The experiments in human lung cancer specimens. (A) Autoradiography, General H&E and immunofluorescence (IF), local H&E and immunohistochemistry (IHC) results of tumor samples from four NSCLC patients (numbered as case 1-4) and one normal lung tissue. The scale bars of General H&E and IF, 2000 μm. The scale bars of local H&E and IHC, 50 μm. (B) The high-resolution CT images of the four NSCLC patients. Arrows indicate the location of tumors. (C) Western blot analysis of tumor samples from the four NSCLC patients and one normal lung tissue (N).

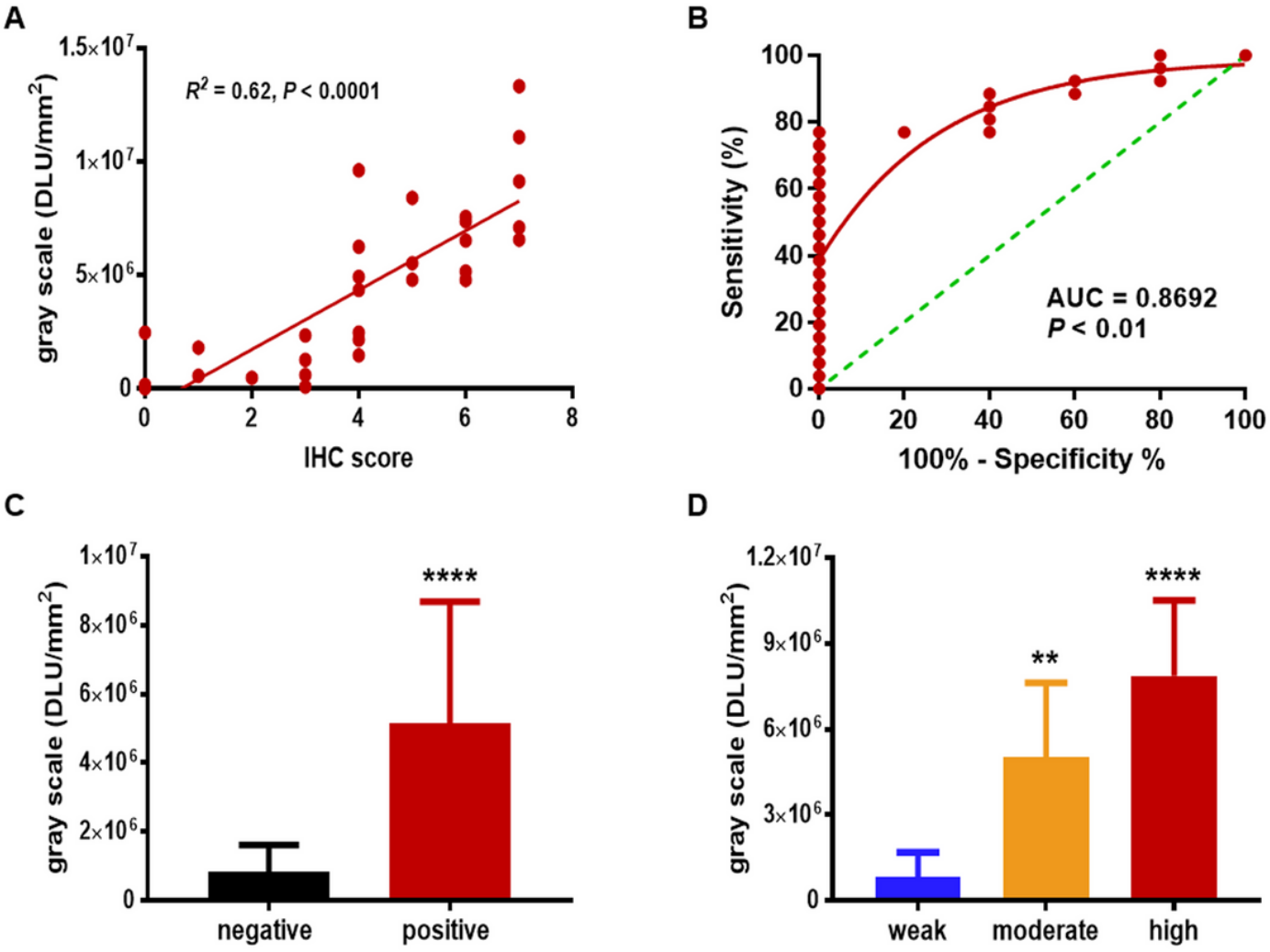

Figure 5

Correlation between 68Ga-NOTA-ZEGFR:1907 uptake and EGFR expression status in human solid tumor samples. (A) Correlation between gray scale value of autoradiography and EGFR immunohistochemical score. (B) Receiver operating characteristic (ROC) curve representing the sensitivity and specificity of 68Ga-NOTA-ZEGFR:1907 gray scale value for predicting the presence of EGFR expression status in patient samples [area under the curve (AUC) = 0.8692, P < 0.01]. (C) The gray scale values of EGFR-expressing negative and positive group. (D) The gray scale values of EGFR expression between weak, moderate, and high positive group. **: P < 0.01; ****: P < 0.0001.

Supplementary Files

This is a list of supplementary files associated with this preprint. Click to download.

- supplementary.docx